SCIENTIFIC CULTURE
www.sci-cult.com

SCIENTIFIC CULTURE, Vol. 11, No. 4, (2025), pp. 2970-2983
Open Access. Online & Print

DOI: 10.5281/zenodo.11425121

ANALYTICAL AND NUMERICAL STUDY OF MHD PULSATILE BLOOD FLOW IN A CATHETERISED POROUS ARTERY WITH DIFFERENT STENOSIS MAGNITUDES UNDER PERIODIC ACCELERATION AND SLIP CONDITIONS

Priyanga R[1], Girija Bai H[2] and Prasanna Jeyanthi M[3]

[1]Research Scholar, Mathematics Department, Sathyabama Institute of Science and Technology, Chennai, India, Email: priyangaravi6@gmail.com
[2]Assistant Professor, Mathematics Department, Sathyabama Institute of Science and Technology, Chennai-119, India
[3]Assistant Professor, Mathematics Department, SRM Institute of Science and Technology Ramapuram, Ramapuram, Chennai, India

Received: 07/11/2025
Accepted: 22/11/2025

Corresponding Author: Priyanga R (priyangaravi6@gmail.com)

ABSTRACT

The Catheterisation is a minimally invasive procedure using thin, flexible tubes to diagnose and manage cardiovascular diseases, particularly in stenosed arteries. This study presents analytical and numerical investigations of pulsatile blood flow influenced by magnetohydrodynamic (MHD) effects in a porous, stenosed artery containing a centrally positioned catheter. The stenosis is considered axially non-uniform and radially symmetric, with the flow subjected to periodic body acceleration and a magnetic field applied perpendicular to the flow direction. The arterial wall is assumed permeable with velocity slip, while blood is treated as a Newtonian and incompressible fluid. Analytical solutions are derived through perturbation techniques, employing modified Bessel functions and matrix inversion. A three-dimensional simulation is also performed using ANSYS Fluent to validate the analytical results. Flow characteristics such as fluid axial velocity, shear stress, volumetric flow rate and resistance impedance are examined under varying magnetic and physiological conditions. The graphical results reveal the combined effects of stenosis geometry, catheter presence, wall slip, and magnetic field on the flow characteristics. These findings provide valuable insights for enhancing catheter-based cardiovascular interventions and demonstrates how MHD-based control can improve energy efficiency in blood flow regulation, potentially supporting the development of energy-aware biomedical devices and self-powered catheter systems.

KEYWORDS: ANSYS Fluent Catheter, MHD, Porous Artery, Pulsatile Flow, Stenosis.

1. INTRODUCTION

Globally, cardiovascular disorders rank among the top causes of death, with arterial stenosis being a common condition where the artery narrows due to plaque buildup. Such constriction limits blood circulation and elevates the likelihood of cardiac arrest and stroke. Catheterisation is a widely used, less invasive technique for diagnosing and treating such conditions by inserting a flexible tube into the artery. However, the presence of the catheter significantly alters blood flow, especially in stenosed arteries.

Blood flow in arteries is naturally pulsatile and can be influenced by external factors such as body acceleration and magnetic fields, particularly during magnetic-based medical procedures. Since blood is electrically conducting, it interacts with magnetic fields, leading to magnetohydrodynamic (MHD) effects. These effects become more complex in porous arteries where the vessel wall allows fluid movement and includes slip conditions at the boundaries.

In recent years, catheterisation has been widely used in real-time applications such as angioplasty, stent placement, cardiac ablation, and targeted drug delivery, particularly for treating coronary artery disease and arrhythmias under image-guided systems like fluoroscopy and MRI.

Recent advancements in catheterisation techniques have demonstrated remarkable clinical efficiency. For instance, in May 2025, Arneja Heart Hospital in Nagpur performed three transcatheter aortic valve replacement (TAVR) procedures in one day with patients remaining conscious and being discharged within 24 hours. This underscores the growing potential of minimally invasive, energy-optimized interventional procedures.

(Akbar et al.2016) discussed numerical and analytical study of two-layered unsteady blood flow through catheterized artery. (Ashfaq and Sohail 2017) gives the shape effect of Cu-nanoparticles in unsteady flow through curved artery with catheterized stenosis. (Daineko et al.2025) define the blood flow numerical modeling in catheterized arteries with mild stenosis. (Eldesoky 2012) determined the slip effects on the unsteady MHD pulsatile blood flow through porous medium in an artery under the effect of body acceleration. (Girija bai et al. 2022) determined the blood Flow in arteries with stenoses: A three-dimensional unsteady flow. (Giulia et al. 2024) demonstrate the cardiac catheterization in pulmonary arterial hypertension: Tips and tricks to enhance diagnosis and guide therapy. (Kabir, Alam, and Uddin 2021) define the numerical simulation of pulsatile blood flow: a study with normal artery, and arteries with single and multiple stenosis. (Keslerová 2023) develops the numerical modeling of generalized Newtonian fluids flow in S-type geometry of bypass. (Kuldeep 2024) investigating the Hemodynamic Changes in Stenosed Arteries with and without Catheter Insertion.

(Mohammad Owais, Usmani, and Muralidhar 2025) given the pulsatile flow hemodynamics in stenosed arterial curvatures. (Mustapha 2008) develops the unsteady response of blood flow through a couple of irregular arterial constrictions to body acceleration.

(Park, Aycan, and Kadem 2025) gives the numerical investigation of the flow induced by a transcatheter intra-aortic entrainment pump. (Prasanna Jeyanthi, and Ganesh 2023) discussed the numerical solution of magnetohydrodynamic flow through duct with perturbated boundary using RBF-FD method. (Paul et. al. 2024) gives the demonstration of angioplasty using a balloon catheter in tetra-hybrid nano-bloodstream within an electrified stenotic arterial cavity under a magnetic field: Artificial neural network analysis. (Sarker, Chatzizisis, and Terry 2020) discussed about the computational optimization of a novel atraumatic catheter for local drug delivery in coronary atherosclerotic plaques.

(Srivastava, and Rastogi 2010) introduced the blood flow through a stenosed catheterized artery: Effects of hematocrit and stenosis shape. (Shafi Ullah Siddiqui, and Chhama Awasthi 2023) introduced the mathematical analysis on pulsatile flow through a catheterized stenosed artery. (Shaikh et al. 2023) gives the comparative analysis of numerical simulations of blood flow through the segment of an artery in the presence of stenosis. (Tian et al. 2016) discussed about the Influence of catheter insertion on the hemodynamic environment in coronary arteries. (Tomaszewski et al. 2020) deals with the experimental and numerical flow analysis through arteries with stent using particle image velocimetry and computational fluid dynamics method.

The novelty of this work lies in the combined analytical and numerical investigation of unsteady MHD pulsatile blood flow through a porous, catheterised artery with axially varying stenosis under periodic body acceleration and velocity slip at permeable walls. To the best of our knowledge, no previous study has simultaneously incorporated these multiple interacting physical effects such as magneto-hydrodynamics, porosity, wall slip and catheter-induced geometric constriction—within a single unified analytical–computational framework. The analytical solution is derived using a modified Bessel-based perturbation technique with matrix inversion, and its validity is confirmed through

three-dimensional transient ANSYS Fluent simulations, establishing strong correlation between theory and computation.

Unlike earlier models that focused on isolated factors such as MHD flow, porosity or single stenosis geometry, this study offers a comprehensive mechanistic understanding of how these parameters jointly influence velocity distribution, shear stress, volumetric flow rate and resistance impedance. The findings provide new insights into magnetic flow regulation and slip-assisted flow enhancement, which are relevant for the design of magnetically guided, energy-efficient catheters and smart vascular devices used in minimally invasive cardiovascular therapies.

2. ANALYTICAL MODELING

The present study focuses on analysis of unsteady blood flow within a catheterized, axisymmetric stenosed artery, where different stenosis magnitudes are considered along the arterial segment.

The artery is modeled as a cylindrical, porous, radially symmetric domain with a central catheter positioned centrally along its longitudinal axis. The wall is treated as permeable and allows partial fluid movement due to slip conditions at the boundary.

Assumptions

To develop the analytical formulation of the proposed model and obtain a tractable mathematical solution, the following physical and mathematical assumptions are made:

- The blood flow is axisymmetric, laminar, unsteady and fully developed within the arterial segment.
- The artery is represented as a **porous cylindrical tube** containing a **rigid, concentric catheter** placed along its central axis.
- The stenosis is mild, axially non-uniform and radially symmetric, allowing the application of a perturbation expansion in terms of the small parameter $\delta \ll 1$.
- Blood is assumed to be a Newtonian, incompressible and electrically conducting fluid with constant density and viscosity.
- The magnetic Reynolds number is considered small so that the induced magnetic field can be neglected relative to the externally applied transverse magnetic field.
- The arterial wall is permeable and satisfies a velocity-slip boundary condition that accounts for the influence of wall porosity and micro-scale effects.
- The catheter surface is rigid and impermeable and therefore obeys a no-slip boundary condition.
- The flow is driven by a time-dependent pressure gradient, and a periodic body acceleration acts along the axial direction to represent physiological motion.
- Thermal and buoyancy effects are neglected, as the flow behavior is primarily governed by hydrodynamic and electromagnetic interactions.

These assumptions provide a realistic yet simplified representation of magnetohydrodynamic pulsatile blood flow through a catheterised porous artery and form the basis for deriving the governing equations of motion presented in the following section.

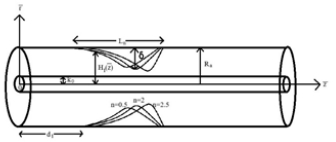

Figure 1: Geometry of the Different Magnitude Stenosis with Catheter.

The axisymmetric geometry with different stenosis magnitudes is based on the work of (Lukendra, Nazibuddin and Karabi Dutta 2018)

$$H(\bar{z}) = \begin{cases} R_a - P\left[L_n^{n-1}\left(z-d_1\right) - \left(z-d_1\right)^n\right], & d_1 \le z \le d_1 + L_n \\ R_a, & otherwise \end{cases} \quad (1)$$

where $L_n \rightarrow$ stenosis length, $\overline{d_1} \rightarrow$ its location, $R_a \rightarrow$ artery radius, $n \ge 2$ stenosis shape (a symmetric stenosis is formed when the shape parameter n=2), $P = \dfrac{\delta\, n^{\frac{n}{n-1}}}{L_n^n\left(n-1\right)}$,

δ the peak elevation of the stenosis, which occurs at $\bar{z} = \dfrac{\overline{d_1} + L_n}{n^{\frac{n}{n-1}}}$ å $\dfrac{\delta}{R_a} << 1$.

In the case of low Reynolds number flow through a mildly stenosed tube, the radial velocity is found to be very small and is often considered negligible.

The momentum equation defining the flow characteristics in cylindrical polar coordinates is expressed as follows:

$$\rho\left(\frac{\partial u_z}{\partial t}\right) = -\frac{\partial p}{\partial z} + \mu\left[\frac{\partial^2 u_z}{\partial r^2} + \frac{1}{r}\frac{\partial u_z}{\partial r}\right] + \rho G - \frac{\mu}{k}u_z + \bar{J} \times \overline{M_0} \quad (2)$$

Based on Maxwell's and Ohm's law assumptions for low magnetic Reynolds number, the Lorentz force simplifies to:

$$\overline{J} \times \overline{M_0} = -\sigma M_0^2 u_z \qquad (3)$$

The boundary conditions are

$$u_0 = 1,\ u_1 = 0 \mid r = k_0$$
$$u_0 = u_s,\ u_1 = 0 \mid r = H(\bar{z}) \qquad (4)$$

Non-dimensional variables are introduced below:

$$r = \bar{r}R_a,\ \ z = \bar{z}R_a,\ \ t = \frac{\bar{t}R_a}{V_a},\ \ u_z = \overline{u_z}\,V_a,\ \ G = \frac{G\,V_0^2}{R_a},$$
$$p = \bar{p}\,\rho\,V_a^2,\ \ \overline{R_n} = \frac{\rho V_a R_a}{\mu},\ \ \overline{M_n^2} = \frac{R_a^2\sigma M_a^2}{\mu},\ \ k_0 = k_0 R_a,$$
$$u_s = \overline{u_s}V_a,\ \ H(\bar{z}) = H_1(\bar{z})R_a,\ \ P = \frac{P}{R_a^{n-1}}, d_1 = \overline{d_1}R_a \qquad (5)$$

The expressions for the dimentionless pressure gradient and body acceleration can be written as:

$$\frac{\partial \bar{p}}{\partial \bar{z}} = f\left(1 + \epsilon e^{i\omega \bar{t}}\right)$$
$$G = g_0 Cos\left(\omega_f \bar{t}\right) \qquad (6)$$

where, $\bar{p} \rightarrow$ pressure, $g_0 \rightarrow$ amplitude of body acceleration, $\omega \rightarrow$ angular frequency of blood flow, $\omega_f \rightarrow$ the angular frequency of body acceleration, $\bar{t} \rightarrow$ time.

The non-dimensional representation of the stenosis geometry is:

$$H_1(\bar{z}) = \begin{cases} 1 - P\left[L_n^{n-1}\left(\bar{z} - \overline{d_1}\right) - \left(\bar{z} - \overline{d_1}\right)^n\right], & \overline{d_1} \le \bar{z} \le \overline{d_1} + L_n \\ 1, & otherwise \end{cases} \qquad (7)$$

By substituting the dimensionless parameters (5) into equations (2) and (4), the non-dimensional governing equation along with the boundary conditions is obtained as:

$$\overline{R_n}\left(\frac{\partial \overline{u_z}}{\partial \overline{t}}\right) = -f\left(1 + \grave{o}e^{i\omega \bar{t}}\right)\overline{R_n} + \frac{\partial^2 \overline{u_z}}{\partial \overline{r}^2} + \frac{1}{\overline{r}}\frac{\partial \overline{u_z}}{\partial \overline{r}} + G\overline{R_n} - \frac{1}{k_0}\overline{u_z} - \overline{M_n}^2\overline{u_z} \qquad (8)$$

$$\overline{u_0} = 1, \quad \overline{u_1} = 0 \mid \bar{r} = k_0$$

$$\overline{u_0} = \overline{u_s}, \quad \overline{u_1} = 0 \mid \bar{r} = H_1(\bar{z}) \qquad (9)$$

The governing equation of motion is a nonlinear partial differential equation. To solve it, we assume a solution of the form:

$$\overline{u_z} = \overline{u_0(r)} + \grave{o}e^{i\omega \bar{t}}\,\overline{u_1(r)} \qquad (10)$$

On substituting equation (10) in equation (8) and by collecting like powers of ò, the zeroth-order and first-order equations are derived.

3. METHOD OF SOLUTION

Zeroth-Order

$$\overline{R_n}\left(f - G\right) = \frac{\partial^2 \overline{u_0(r)}}{\partial \overline{r}^2} + \frac{1}{\overline{r}}\frac{\partial \overline{u_0(r)}}{\partial \overline{r}} - \left(\frac{1}{k_0} + \overline{M_n}^2\right)\overline{u_0(r)} \qquad (11)$$

First-Order

$$f\overline{R_n} = \frac{\partial^2 \overline{u_1(r)}}{\partial \overline{r}^2} + \frac{1}{\overline{r}}\frac{\partial \overline{u_1(r)}}{\partial \overline{r}} - \left(\frac{1}{k_0} + \overline{M_n}^2 + \overline{R_n} i\omega\right)\overline{u_1(r)} \qquad (12)$$

Equation (11) and (12) is identified as a modified Bessel's differential equations and its solution can be written as

$$\overline{u_0(r)} = S_1 I_0(\lambda_1 \overline{r}) + S_2 K_0(\lambda_1 \overline{r}) + f_2 \qquad (13)$$
$$\overline{u_1(r)} = S_3 I_0(\lambda_2 \overline{r}) + S_4 K_0(\lambda_2 \overline{r}) + f_3 \qquad (14)$$

Here, I_0 and K_0 are modified Bessel functions of the 1st and 2nd kind respectively. Here, λ_1 and λ_2 are defined as:

$$\lambda_1^2 = \frac{1}{k_0} + \overline{M_n}^2,\ \lambda_2^2 = \frac{1}{k_0} + \overline{M_n}^2 + \overline{R_n} i\omega$$

and the particular solutions arising due to the non-homogeneous terms are:

$$f_2 = -\frac{\overline{R_n}(f-G)}{\lambda_1^2},\ f_3 = -\frac{f\overline{R_n}}{\lambda_2^2}$$

To determine the unknown constants S_1, S_2, S_3, S_4 appropriate boundary conditions are imposed at the arterial wall and at the catheter interface. Substituting the boundary conditions given in equation (9) into equations (13) and (14) yields a set of simultaneous linear equations. These equations are systematically arranged into a matrix form, which is then solved using the matrix inversion method. This approach facilitates an accurate and consistent evaluation of the constants governing the radial variation of the velocity components.

$$S_1 = \frac{(1-f_2)K_0(\lambda_1 H_1(\bar{z})) - (\overline{u_s} - f_2)K_0(\lambda_1 k_0)}{I_0(\lambda_1 k_0)K_0(\lambda_1 H_1(\bar{z})) - K_0(\lambda_1 k_0)I_0(\lambda_1 H_1(\bar{z}))}$$

$$S_2 = \frac{-(1-f_2)I_0(\lambda_1 H_1(\bar{z})) + (\overline{u_s} - f_2)I_0(\lambda_1 k_0)}{I_0(\lambda_1 k_0)K_0(\lambda_1 H_1(\bar{z})) - K_0(\lambda_1 k_0)I_0(\lambda_1 H_1(\bar{z}))}$$

$$S_3 = \frac{-f_3 K_0(\lambda_1 H_1(\bar{z})) + f_3 K_0(\lambda_1 k_0)}{I_0(\lambda_1 k_0)K_0(\lambda_1 H_1(\bar{z})) - K_0(\lambda_1 k_0)I_0(\lambda_1 H_1(\bar{z}))}$$

$$S_4 = \frac{f_3 I_0(\lambda_1 H_1(\bar{z})) - f_3 I_0(\lambda_1 k_0)}{I_0(\lambda_1 k_0)K_0(\lambda_1 H_1(\bar{z})) - K_0(\lambda_1 k_0)I_0(\lambda_1 H_1(\bar{z}))}$$

Thus, the general solution is expressed in the following form:

$$\overline{u_z} = S_1 I_0(\lambda_1 \bar{r}) + S_2 K_0(\lambda_1 \bar{r}) + f_2 + \grave{o}e^{i\omega\bar{t}}\left(S_3 I_0(\lambda_2 \bar{r}) + S_4 K_0(\lambda_2 \bar{r}) + f_3\right) \quad (15)$$

Shear stress

$$\tau_w = -\frac{\partial \overline{u_z}}{\partial \bar{r}} | \bar{r} = H_1(\bar{z})$$

$$\tau_w = -\left[\lambda_1 S_1 I_1(\lambda_1 H_1(\bar{z})) - \lambda_1 S_2 K_1(\lambda_1 H_1(\bar{z})) + \grave{o}e^{i\omega\bar{t}}\left(S_3 I_1(\lambda_2 H_1(\bar{z})) - S_4 K_1(\lambda_2 H_1(\bar{z}))\right)\right] \quad (16)$$

Shear stress gradient

$$\frac{\partial \tau_w}{\partial \bar{t}} - \grave{o}e^{i\omega\bar{t}} i\omega\lambda_2\left(S_3 I_1(\lambda_2 H_1(\bar{z})) - S_4 K_1(\lambda_2 H_1(\bar{z}))\right) \quad (17)$$

Volumetric flow rate

$$Q_v = 2\Pi\int_0^{H_1(\bar{z})} \bar{r}\,\overline{u_z}\,d\bar{r}$$

$$Q_v = 2\Pi\left[S_1\left(\frac{H_1(\bar{z})}{\lambda_1}\right)I_1(\lambda_1 H_1(\bar{z})) - S_2\left(\frac{H_1(\bar{z})}{\lambda_1}\right)K_1(\lambda_1 H_1(\bar{z})) + f_2\frac{H_1(\bar{z})^2}{2}\right]$$
$$+2\Pi\grave{o}e^{i\omega\bar{t}}\left[S_3\left(\frac{H_1(\bar{z})}{\lambda_2}\right)I_1(\lambda_2 H_1(\bar{z})) - S_4\left(\frac{H_1(\bar{z})}{\lambda_2}\right)K_1(\lambda_2 H_1(\bar{z})) + f_3\frac{H_1(\bar{z})^2}{2}\right] \quad (18)$$

Resistance impedance

$$R_\lambda = \frac{\Delta\bar{p}}{Q_v}$$

$$R_\lambda = f\left(1+\grave{o}e^{i\omega\bar{t}}\right)\frac{1}{2\Pi\left[S_1\left(\frac{H_1(\bar{z})}{\lambda_1}\right)I_1\left(\lambda_1 H_1(\bar{z})\right)-S_2\left(\frac{H_1(\bar{z})}{\lambda_1}\right)K_1\left(\lambda_1 H_1(\bar{z})\right)+f_2\frac{H_1(\bar{z})^2}{2}\right]}$$
$$\frac{1}{+2\Pi\grave{o}e^{i\omega\bar{t}}\left[S_3\left(\frac{H_1(\bar{z})}{\lambda_2}\right)I_1\left(\lambda_2 H_1(\bar{z})\right)-S_4\left(\frac{H_1(\bar{z})}{\lambda_2}\right)K_1\left(\lambda_2 H_1(\bar{z})\right)+f_3\frac{H_1(\bar{z})^2}{2}\right]} \quad (19)$$

4. COMPUTATIONAL APPROACH

To validate the analytical model and visualize hemodynamic behavior, a three-dimensional transient simulation was carried out using ANSYS Fluent (v25.1). The computational study focused on MHD pulsatile blood flow through a porous, catheterized artery featuring a single cosine-shaped stenosis with shape parameter $n = 2$. The artery geometry was modeled as a cylindrical domain with a centrally inserted catheter and permeable walls.

Physics Setup

The simulation considered blood as an incompressible, Newtonian, electrically conducting fluid, and assumed laminar flow. The following effects were implemented using User Defined Functions (UDFs):

- Pulsatile inlet velocity to replicate physiological cardiac cycles.
- Magnetic body force (Lorentz force) in the x-direction to model MHD effects.

The artery wall was treated as a porous zone using viscous resistance coefficients to reflect permeable boundary effects and the catheter wall was modeled as a rigid, no-slip boundary.

Solver And Mesh Details

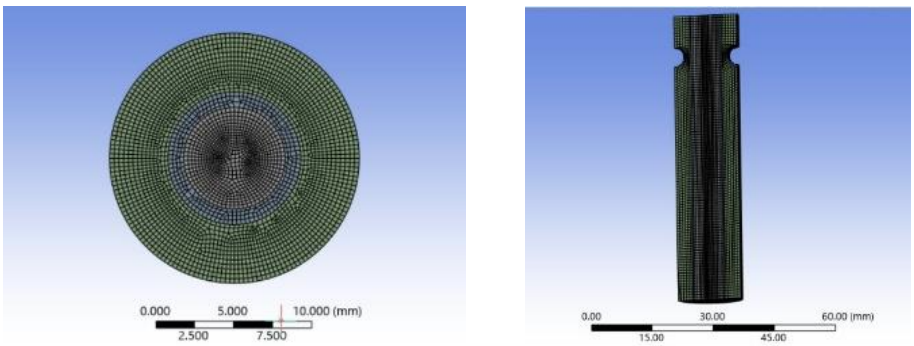

(a) Mesh (b) Cross-section

Figure 2: Figures of Mesh at Right View and Cross Section.

- Solver type: Pressure-based, transient
- Viscous model: Laminar
- Time stepping: 1 s time step, 10 steps total
- Pressure–velocity coupling: SIMPLE
- Discretization schemes: Second-order upwind for momentum, second-order for pressure
- Porous zone settings: Porosity = 0.7, Viscous resistance = $2.111\times10^{8}\,m^{-2}$

The mesh contained approximately 170,000 cells, with orthogonal quality ≥ 0.07 and maximum aspect ratio ≤ 28.5, ensuring acceptable accuracy.

Post-Processing and Results

From the Fluent simulations Figure 3 to 6, two key flow variables were extracted:

- Axial velocity and Shear stress contours to visualize the flow distribution for different k_0 and $\overline{M_0}$,
- XY plots along the artery wall to evaluate frictional forces exerted by the fluid.

The results showed that:

(from Figures 7 and 8)

- Increasing k_0 (larger catheter) narrowed the flow passage, reducing axial velocity and increasing Shear stress.
- Increasing $\overline{M_0}$ led to stronger Lorentz damping, decreasing central flow velocity and shifting velocity gradients toward the wall, thereby increasing τ_w.

The simulations achieved convergence within 20 iterations per time step and showed strong agreement with analytical trends, validating the perturbation-based solution.

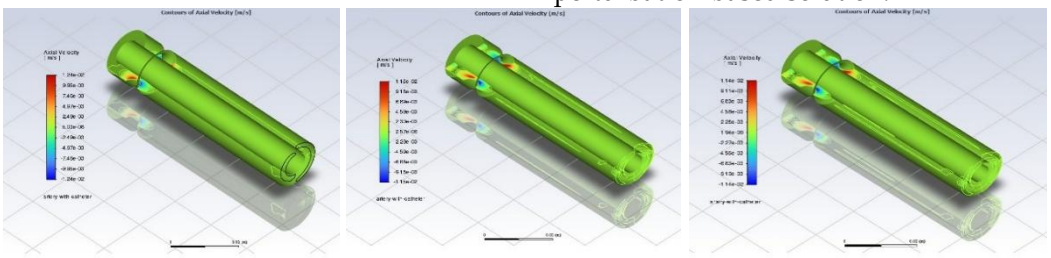

(a) Contour of axial velocity for $k_0 = 0.2$ (b) Contour of axial velocity for $k_0 = 0.5$ (c) Contour of axial velocity for $k_0 = 0.7$

Figure 3: Variation Of Axial Velocity Contours with Catheter Radius Values $k_0 = 0.2, 0.5, 0.7$.

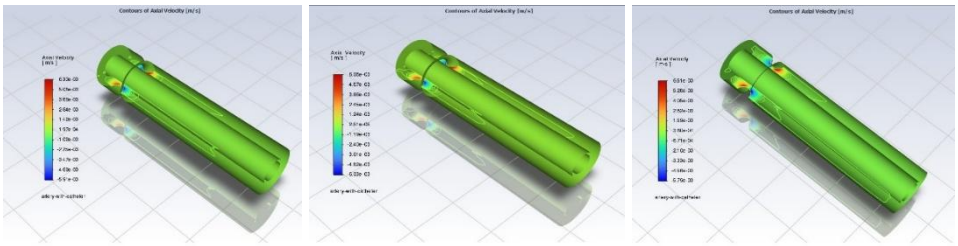

(a) Contour of axial velocity for $M_n = 10$ (b) Contour of axial velocity for $\overline{M_n} = 30$ (c) Contour of axial velocity for $\overline{M_n} = 40$

Figure 4: Variation Of Axial Velocity Contours with Magnetic Parameter Values $M_n = 10, 30, 40$.

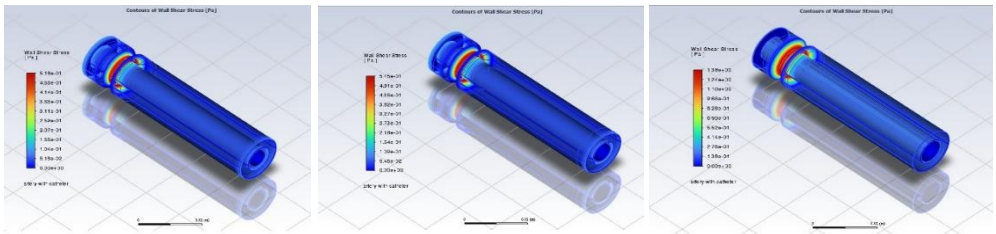

(a) Contour of shear stress for $k_0 = 0.2$ (b) Contour of shear stress for $k_0 = 0.5$ (c) Contour of shear stress for $k_0 = 0.7$

Figure 5: Comparison Of Shear Stress Contours at Various Catheter Radius Conditions $k_0 = 0.2, 0.5, 0.7$.

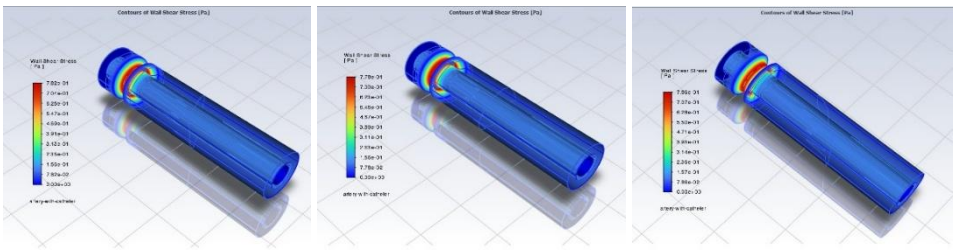

(a) Contour of Shear stress for $M_n = 10$ (d) Contour of Shear stress for $\overline{M_n} = 30$ (e) Contour of Shear stress for $\overline{M_n} = 40$

Figure 6: Comparison of Shear Stress Contours at Various Magnetic Parameter Conditions $M_n = 10, 30, 40$.

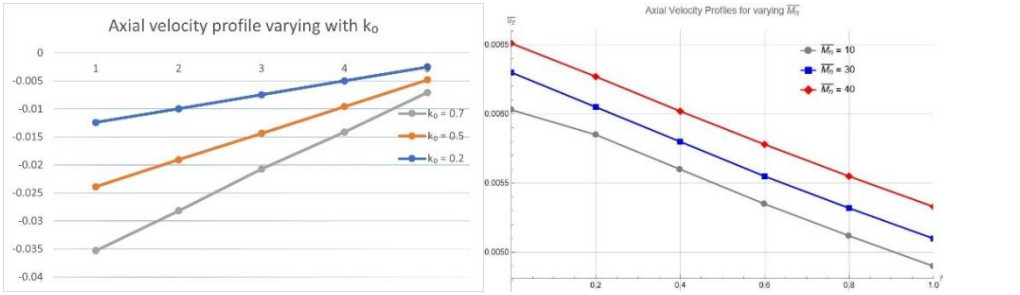

(a) Velocity drops with increasing K_0 (b) Reduction in axial velocity with higher $\overline{M_n}$

Figure 7: Graphs Showing the Effect of Varying Catheter Radius $k_0 = 0.2, 0.5, 0.7$ ***And Magnetic Parameter*** $\overline{M_n} = 10, 30, 40$ ***On Axial Velocity.***

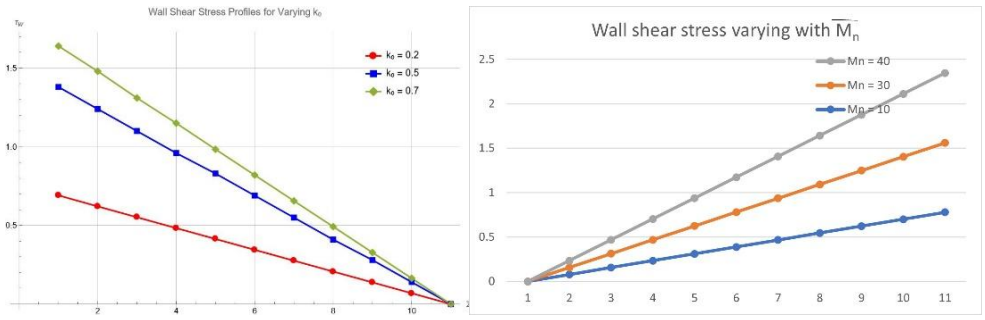

(a) Shear Stress rises with higher K_0 (b) Greater $\overline{M_n}$ elevates Shear stress

Figure 8: Graphs Showing the Effect of Varying Catheter Radius $k_0 = 0.2, 0.5, 0.7$ ***And Magnetic Parameter*** $\overline{M_n} = 10, 30, 40$ ***On Shear Stress.***

5. RESULTS AND DISCUSSION

In this investigation, blood flow through a catheterized artery is examined, with the stenosis depth maintained at 30% percent of the arterial radius. The analysis considers the combined influence of slip velocity and different magnitudes of the stenosis shape on various hemodynamic parameters. The magnitude of the stenosis is varied using shape parameter "$n = 0.5, 2, 2.5$". For each case, two slip velocity conditions are explored: $\overline{u_s} = 0$ (no-slip) and $\overline{u_s} = 3$ (slip). The results include detailed evaluations of axial velocity, Shear stress, volumetric flow rate and Resistance impedance. Catheter insertion induces notable changes in flow behaviour and the study highlights how variations in stenosis shape and wall slip affect the overall dynamics of blood flow through the porous artery.

Figures 9a to 9c reveal that the flow within the annular region is significantly influenced by the aspect ratio k_0, expressed as the ratio of the catheter radius and the arterial radius. As k_0 increases, the effective cross-sectional area available for flow decreases, leading to greater surface resistance and a noticeable reduction in flow velocity throughout the annular region.

Figures 9d to 9f demonstrate that increasing the magnetic field strength $\overline{M_n}$ leads to a significant reduction in flow velocity, thereby decreasing the velocity gradient within the channel.

Figures 9g to 9i illustrate that as the Reynolds number $\overline{R_n}$ increases, corresponding to a rise in catheter speed, likewise the axial velocity of the flow rises under both slip and no-slip arterial wall conditions. The presence of slip at the arterial boundary enhances the flow velocity compared to the no-slip condition. This influence of wall slip is

more significant at lower $\overline{R_n}$, while its effect gradually diminishes as the $\overline{R_n}$ increases.

Figures 10a to 10c illustrate that the Shear stress increases with a rise in catheter radius k_0 because the flow area gets smaller, causing more friction at the walls. As the magnetic parameter $\overline{M_n}$ increases, the magnetic force slows the flow in the centre and pushes it toward the walls, which also raises the Shear stress as indicated in figures 10d to 10f. On the other hand, when the Reynolds number $\overline{R_n}$ increases, the flow becomes faster and smoother, which reduces the Shear stress near the walls, as illustrated in figures 10g to 10i.

Figures 11a to 11c show that the volumetric flow rate reduces when the catheter radius k_0 is increased, since the reduced flow area leads to higher resistance. In Figures 11d to 11f, increasing the magnetic parameter $\overline{M_n}$ also reduces the flow rate due to the magnetic damping effect. However, as seen in Figures 11g to 11i, the Reynolds number $\overline{R_n}$ has a mixed effect: for stenosis magnitude $n=0.5$, the flow rate increases, but for higher magnitudes $n=2,2.5$, it decreases. This is because although the depth remains the same, higher $_n$ leads to more severe blockage, affecting the flow. The presence of wall slip slightly enhances the flow compared to no-slip conditions.

The variation of resistance impedance with different flow parameters is shown for three stenosis magnitudes n=0.5,2,2.5.

From Figures 12a to 12c, resistance impedance decreases with increasing catheter radius k_0 for all $_n$, with a steeper drop seen at higher $_n$.

Figures 12d to 12f present the effect of magnetic parameter $\overline{M_n}$ on resistance impedance. For n=0.5, resistance impedance decreases with $\overline{M_n}$, as the magnetic field induces Lorentz forces that resist motion. For n=2, the impedance first increases and then slightly decreases, showing a non-monotonic trend due to interaction between magnetic damping and inertial effects. For n=2.5, the impedance initially increases sharply, reaches a peak, and then decreases, indicating that at high magnetic strength, flow stabilization dominates, lowering resistance.

Figures 12g to 12i show the effect of Reynolds number $\overline{R_n}$: $n=0.5$, impedance decreases with $\overline{R_n}$; for $n=2$, it increases; and for $n=2.5$, it slightly decreases then increases notably with $\overline{R_n}$ due to enhanced flow resistance in severe stenosis.

To highlight the relevance and advancement of the present investigation, a comparison with previous analytical, numerical and experimental studies is presented in Table 1.

Earlier research primarily examined isolated effects such as magnetic damping, catheter influence or wall porosity.

In contrast, the present work integrates all these physical mechanisms within a single unified analytical–numerical framework, supported by ANSYS Fluent validation.

This comparative summary demonstrates that the proposed model not only agrees with established trends in the literature but also extends them by incorporating the coupled effects of magnetohydrodynamics, slip velocity, porosity and catheter geometry under periodic acceleration.

Table 1: Comparison Of Present Study with Selected Previous Works.

Reference	Present Study Comparison
Eldesoky (2012)	Reproduces Lorentz damping and slip velocity effects in MHD porous blood flow. The present study extends this by including a concentric catheter, variable stenosis geometry and transient body acceleration effects with 3D numerical validation.
Srivastava & Rastogi (2010)	Confirmed that catheter presence increases wall shear and resistance. The current model incorporates magnetic field influence and wall permeability with slip to analyse electromagnetic control of hemodynamic resistance.
Tomaszewski et al. (2020)	Experimental and CFD analysis showed localized shear enhancement near implants. The present results exhibit similar wall shear behaviour and further reveal how MHD and slip parameters modify these experimental trends.
Daineko et al. (2025)	Reported that catheter-induced narrowing increases pressure drop in mild stenosis. The present model extends this by coupling MHD and porous-slip effects to evaluate flow resistance and damping under magnetic control.
Farooq et al. (2025)	Analysed MHD flow with partial slip and variable permeability, showing slip reduces resistance. The current study adds catheter geometry, stenosis non-uniformity and time-dependent forcing for realistic arterial flow prediction.
Present Study (2025)	Provides a unified analytical–numerical model of pulsatile MHD blood flow in a porous, catheterized stenosed artery under periodic acceleration, incorporating slip and magnetic effects for improved understanding of flow regulation and device optimization.

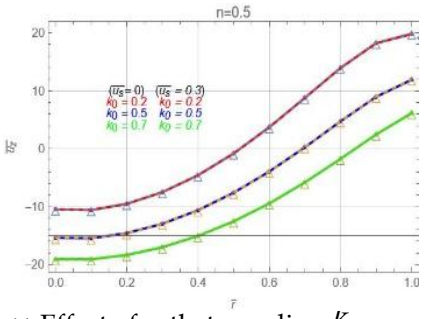

(a) Effect of catheter radius κ_0 on axial velocity at $n = 0.5$, with $R_n = 30$, $G = 0.5$, $\omega = 1$ and $t = 1$.

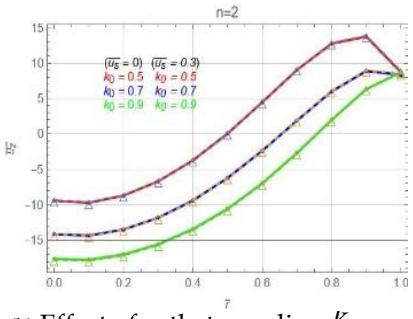

(b) Effect of catheter radius κ_0 on axial velocity at $n = 2$, with $R_n = 30$, $G = 0.5$, $\omega = 1$ and $t = 1$.

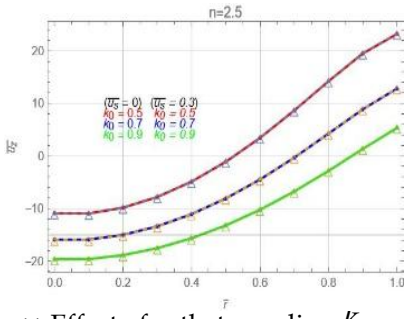

(c) Effect of catheter radius κ_0 on axial velocity at $n = 2.5$, with $R_n = 30$, $G = 0.5$, $\omega = 1$ and $t = 1$.

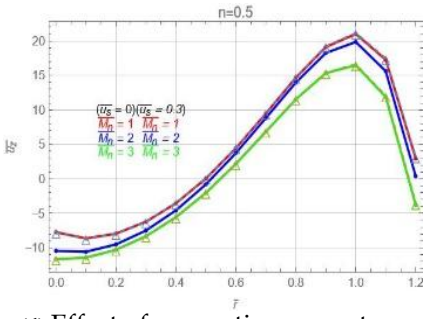

(d) Effect of magnetic parameter M_n on axial velocity at $n = 0.5$, with $R_n = 30$, $G = 0.5$, $\omega = 1$ and $t = 1$.

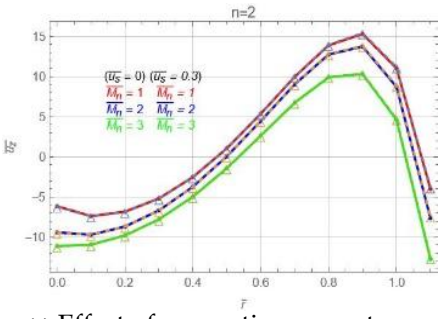

(e) Effect of magnetic parameter M_n on axial velocity at $n = 2$, with $R_n = 30$, $G = 0.5$, $\omega = 1$ and $t = 1$.

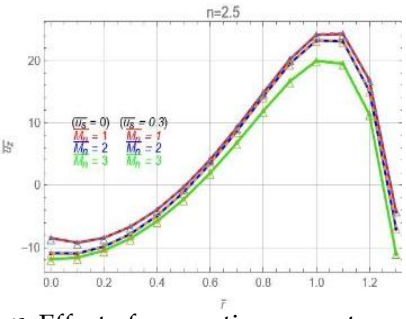

(f) Effect of magnetic parameter M_n on axial velocity at $n = 2.5$, with $R_n = 30$, $G = 0.5$, $\omega = 1$ and $t = 1$.

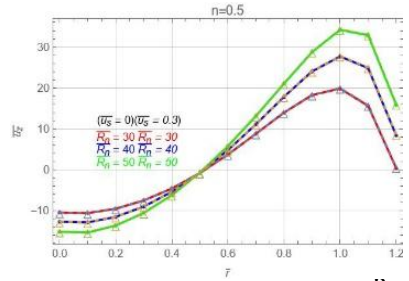

(g) Effect of Reynolds number R_n on axial velocity at $n = 0.5$, with $M_n = 2$, $k_0 = 0.2$, $\omega = 1$ and $t = 1$.

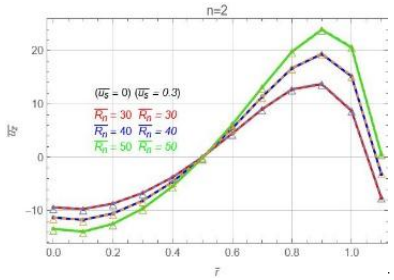

(h) Effect of Reynolds number R_n on axial velocity at $n = 2$, with $M_n = 2$, $k_0 = 0.2$, $\omega = 1$ and $t = 1$.

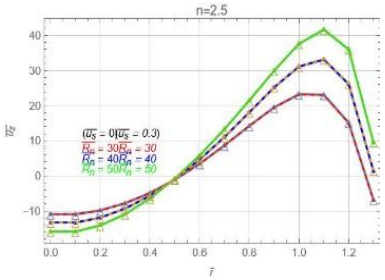

(i) Effect of Reynolds number R_n on axial velocity at $n = 2.5$, with $M_n = 2$, $k_0 = 0.2$, $\omega = 1$ and $t = 1$.

Figure 9: Variation of Axial Velocity Profiles.

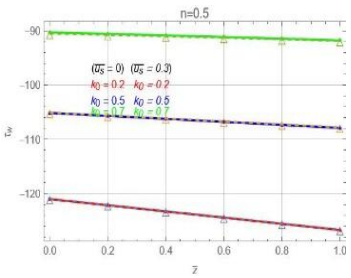

(a) Shear Stress for various catheter radius k_0

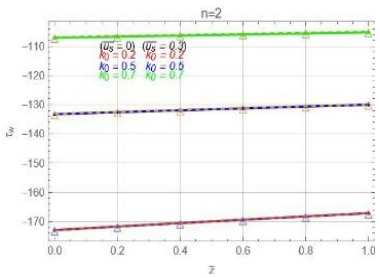

(b) Shear Stress for various catheter radius k_0

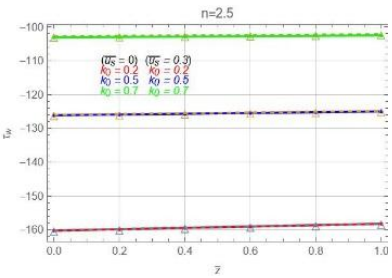

(c) Shear Stress for various catheter radius k_0

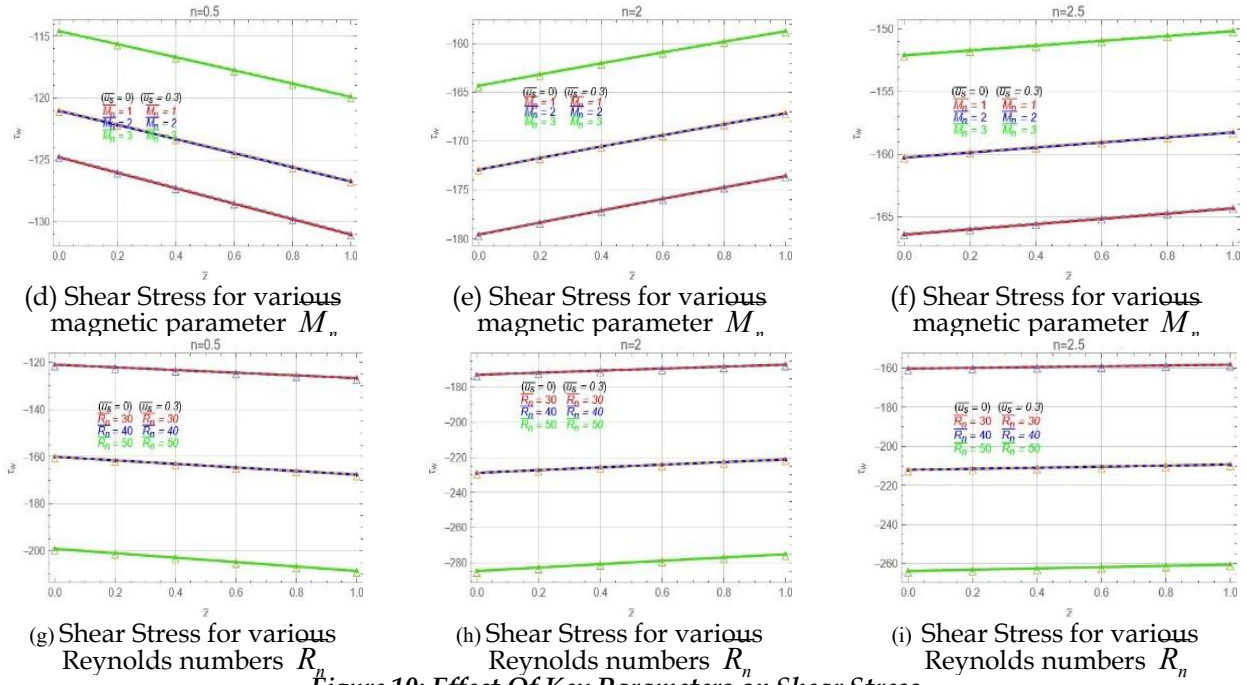

(d) Shear Stress for various magnetic parameter M_n (e) Shear Stress for various magnetic parameter M_n (f) Shear Stress for various magnetic parameter M_n

(g) Shear Stress for various Reynolds numbers R_n (h) Shear Stress for various Reynolds numbers R_n (i) Shear Stress for various Reynolds numbers R_n

Figure 10: Effect Of Key Parameters on Shear Stress.

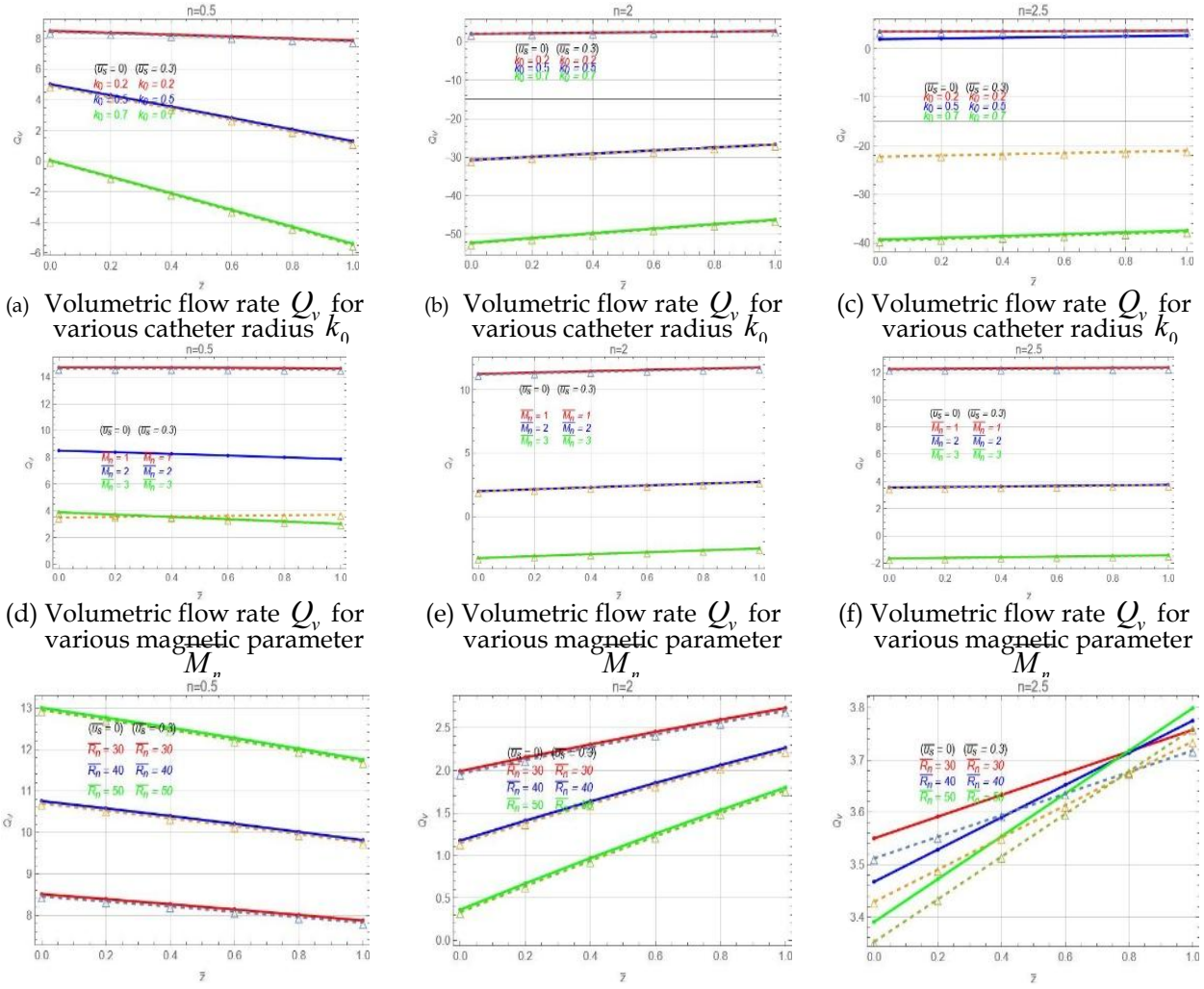

(a) Volumetric flow rate Q_v for various catheter radius k_0 (b) Volumetric flow rate Q_v for various catheter radius k_0 (c) Volumetric flow rate Q_v for various catheter radius k_0

(d) Volumetric flow rate Q_v for various magnetic parameter M_n (e) Volumetric flow rate Q_v for various magnetic parameter M_n (f) Volumetric flow rate Q_v for various magnetic parameter M_n

(g) Volumetric flow rate Q_v for various Reynolds numbers R_n (h) Volumetric flow rate Q_v for various Reynolds numbers R_n (i) Volumetric flow rate Q_v for various Reynolds numbers R_n

Figure 11: Effect Of Key Parameters on Volumetric Flow Rate Q_v.

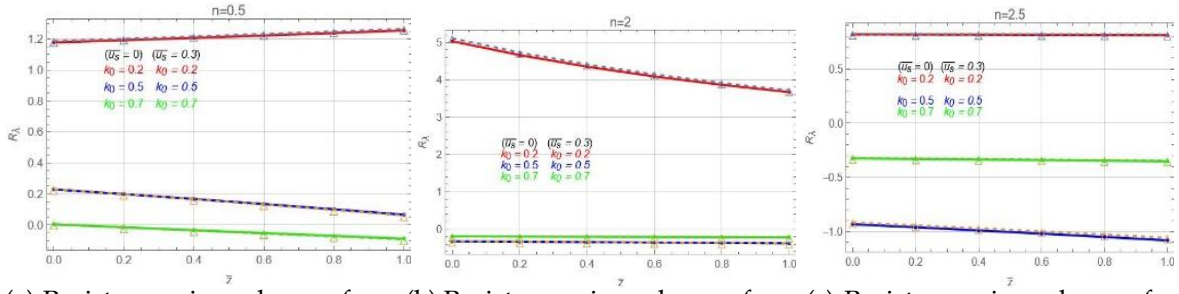

(a) Resistance impedance for various catheter radius k_0 (b) Resistance impedance for various catheter radius k_0 (c) Resistance impedance for various catheter radius k_0

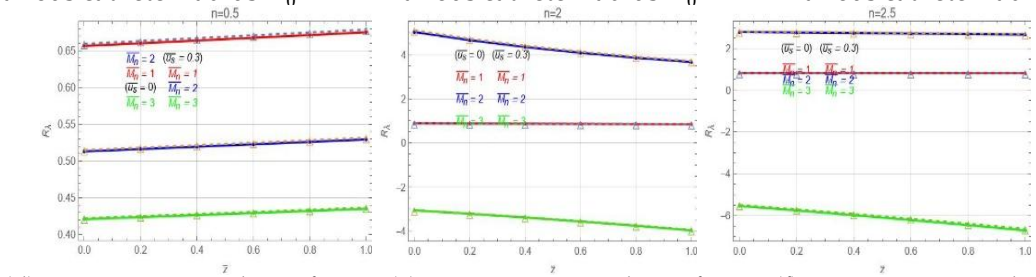

(d) Resistance impedance for various magnetic parameter M_n (e) Resistance impedance for various magnetic parameter M_n (f) Resistance impedance for various magnetic parameter M_n

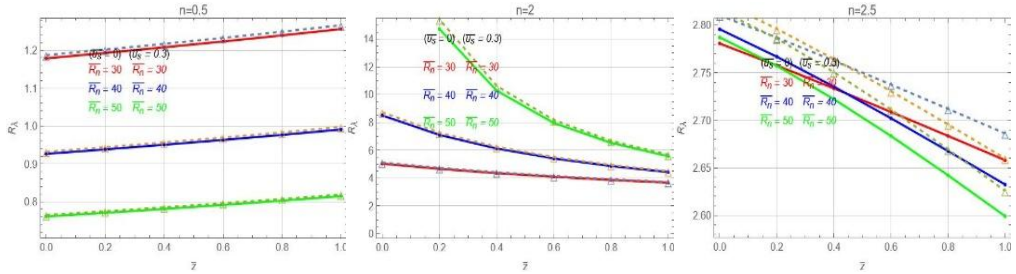

(g) Resistance impedance for various Reynolds numbers R_n (h) Resistance impedance for various Reynolds numbers R_n (i) Resistance impedance for various Reynolds numbers R_n

Figure 12: Flow Resistance Analysis for Different Parameters.

Tables 2 and 3 show the analytical and numerical outcomes for key flow parameters. The close agreement between these results supports the validity of the numerical model and confirms the reliability of the analytical approach.

Table 2: Analytical And Numerical Results of Hemodynamic Parameters Under Varying Physical Conditions.

	K□	M□	R□	$\bar{u}_z$				τ_w				Q_v				R_λ			
A	0.2	2	30	0.05	4.46	9.02	12.73	-170.5	-169.3	-168.2	-167.1	1.99	2.15	2.30	2.45	5.03	4.66	4.35	4.09
A	0.5			-6.21	-2.37	1.87	5.99	-131.9	-131.2	-130.6	-130.0	-30.7	-29.8	-29.0	-28.2	-0.32	-0.33	-0.34	-0.35
A	0.7			-10.5	-6.95	-2.68	1.98	-106.3	-105.9	-105.6	-105.2	-52.2	-50.9	-49.6	-48.4	-0.91	-0.91	-0.20	-0.20
A	0.5	1	30	1.04	5.36	9.95	13.88	-177.1	-175.9	-174.7	-173.5	11.4	11.5	11.6	11.7	5.03	4.66	4.35	4.09
A	0.5	2	30	0.87	0.86	0.86	0.85	-170.5	-169.3	-168.2	-167.1	2.30	2.45	2.59	2.73	4.35	4.09	3.86	3.67
A	0.5	3	30	-1.42	2.63	6.72	9.89	-162.0	-160.9	-159.8	-158.7	-2.97	-2.82	-2.67	-2.53	-3.38	-3.56	-3.75	-3.96
A	0.5	2	40	-0.01	5.43	11.33	16.70	-225.6	-224.1	-222.6	-221.1	1.17	1.40	1.63	1.85	8.50	7.10	6.12	5.41
A	0.5	2	50	-0.15	6.14	13.10	19.79	-280.7	-278.8	-276.9	-275.1	0.36	0.67	0.96	1.25	26.1	14.7	10.2	7.96
N	0.2	2		-.01	-.009	-.007	-.004	1.64	1.48	1.31	1.15								
N	0.5	2		-.011	-.009	-.006	-.004	1.38	1.24	1.10	0.96								
N	0.7	2		-.01	-.009	-.006	-.004	0.69	0.62	0.55	0.48								
N	0.5	10		.006	.005	.005	.005	0.07	0.15	0.23	0.31								
N	0.5	30		.006	.006	.005	.005	0.08	0.16	0.23	0.31								
N	0.5	40		.006	.006	.006	.005	0.079	0.16	0.24	0.31								

Validation

Table 3: Validation Of Analytical and Numerical Results.

Parameter	Analytical Prediction	ANSYS Simulation Result	Outcomes
Axial velocity vs k_0	Decreases	Decreases	☑ Excellent correlation
Axial velocity vs $\overline{M_n}$	Decreases	Decreases	☑ Strong agreement
Shear stress vs k_0	Increases	Increases	☑ Close match
Shear stress vs $\overline{M_n}$	Increases	Increases	☑ Good qualitative match

Summary Of Key Observation

The major parametric trends and model validations derived from both analytical and ANSYS Fluent results are summarised below:

- Axial velocity decreased with increasing k_0 due to reduced flow area — useful for flow control in narrow arterial segments.
- Shear stress increased with k_0 from tighter flow — important for catheter safety and clot prevention.
- Axial velocity decreased with increasing $\overline{M_n}$ due to Lorentz damping — supports external magnetic flow regulation.
- Shear stress increased with $\overline{M_n}$ as flow shifted toward the wall — beneficial for enhancing targeted drug transport.
- Axial velocity increased with higher $\overline{R_n}$ as inertia dominated — relevant in high-pressure blood flow or device-driven circulation.
- Shear stress decreased with higher $\overline{R_n}$ due to smoother velocity distribution — reduces mechanical load on arterial walls.
- ANSYS Fluent results matched analytical trends well, validating the model.

6. CONCLUSION

A comprehensive analytical and numerical investigation of unsteady magnetohydrodynamic (MHD) pulsatile blood flow in a porous, catheterized stenosed artery under periodic body acceleration has been presented. The study demonstrates how electromagnetic, porous and slip effects interact to regulate blood flow characteristics in constricted arterial geometries.

Physically, the results reveal that the magnetic field produces a Lorentz force that suppresses axial velocity and enhances wall shear stress, while velocity slip at the permeable wall counteracts this damping by allowing smoother near-wall motion. The porous structure of the arterial wall contributes additional resistance, moderating the overall flow rate. Stenosis geometry and catheter radius jointly influence the flow acceleration and shear gradients, highlighting the delicate balance between constriction-induced pressure rise and viscous dissipation.

The integration of these coupled effects provides a deeper understanding of how magnetic control and surface slip can be optimized to manage flow resistance in minimally invasive cardiovascular procedures. This framework offers potential applications in the design of energy-efficient, magnetically guided and self-regulating catheter systems that can improve blood transport with reduced mechanical stress on arterial walls.

Future research can extend the present model by incorporating non-Newtonian rheology, wall elasticity and temperature-dependent effects to further enhance physiological accuracy and clinical applicability.

Acknowledgement: The authors declare that there is no acknowledgement for this work.

Data Availability Statement: There is no data availability statement in this manuscript.

Conflict Of Interest: The authors declare that there is no conflict of interest regarding the publication of this paper.

REFERENCES

Akbar, Z., Nasir, A., Sajid, M., and Tasawar, H. 2016. "Numerical and analytical study of two-layered unsteady blood flow through catheterized artery". *PLOS ONE* 11(8). e0161377.

Ashfaq, A., and Sohail, N. 2017. "Shape effect of Cu-nanoparticles in unsteady flow through curved artery with catheterized stenosis". *Results in Physics* 7. 677-689.

Daineko, Y., Alpar, S., Alipova, B., Tokmukhamedova, F. and Bolatov, Z. 2025. "Blood flow numerical modeling in catheterized arteries with mild stenosis". *Mathematics and Computers in Simulation*. 240. 10.1016/j.matcom.2025.07.051.

Eldesoky, I.M. 2012. "Slip effects on the unsteady MHD pulsatile blood flow through porous medium in an artery under the effect of body acceleration". *International Journal of Mathematics and Mathematical Sciences* 2012. 1-26.

Farooq J., Abbas A., Alshammari B.M., Mir A. and Kolsi L. 2025. "Analysis of MHD slip blood flow through a constricted artery filled with a porous medium of variable permeability: Applications in Biomedical Engineering". *Alexandria Engineering Journal*. 114. 426-439.

Girija bai, H., Jeyanthi, M., Palani Hemavathy, Premkumar, M., and Ismail, M. 2022. "Blood Flow in arteries with stenoses: A three-dimensional unsteady flow". *The Journal of Positive Psychology* 6. 3336-3343.

Giulia, G., Kaushiga, K., Andrew, C., and Konstantinos, D. 2024. "Cardiac catheterization in pulmonary arterial hypertension: Tips and tricks to enhance diagnosis and guide therapy". *International Journal of Cardiology Congenital Heart Disease* 17. 100527.

Kabir, Md., Alam, Md., and Uddin, Md., 2021. "Numerical simulation of pulsatile blood flow: a study with normal artery and arteries with single and multiple stenosis". *Journal of Engineering and Applied Science* 68. 10.1186/s44147-021-00025-9.

Keslerová, R. 2023. "Numerical modeling of generalized Newtonian fluids flow in S-type geometry of bypass". *Journal of Computational and Applied Mathematics* 429.

Kuldeep, M., 2024. "Investigating the Hemodynamic Changes in Stenosed Arteries with and without Catheter Insertion". *International Journal of Scientific Research in Science and Technology* 11(6), https://doi.org/10.32628/IJSRST241161122.

Lukendra, K., Nazibuddin, A., and Karabi Dutta C. 2018. "Mathematical Modeling of Blood Flow through an Inclined Axially Non-Symmetric Stenosed Catheterized Artery with Body Acceleration". *International Journal of Applied Engineering Research* 13(21). 15290-15298.

Mohammad Owais, Usmani, A.Y., and Muralidhar, K. 2025. "Pulsatile flow hemodynamics in stenosed arterial curvatures". *Physical Review Fluids* 10. 063101.

Mustapha, N., Chakravarty, S., Mandal, P.K., and Amin, N. 2008 "Unsteady response of blood flow through a couple of irregular arterial constrictions to body acceleration". *Journal of Mechanics in Medicine and Biology* 8. 395–420.

Park, Y., Aycan, O., and Kadem, L. 2025. "Numerical investigation of the flow induced by a transcatheter intra-aortic entrainment pump". *Computer Methods in Biomechanics and Biomedical Engineering* 1–14. https://doi.org/10.1080/10255842.2025.2471517.

Paul P., Karmakar P., Das S. and Das S. 2024 "Demonstration of angioplasty using a balloon catheter in tetra-hybrid nano-bloodstream within an electrified stenotic arterial cavity under a magnetic field: Artificial neural network analysis". *Biomedical Signal Processing and Control* 96. 106549.

Prasanna Jeyanthi, M., and Ganesh, S. 2023. "Numerical solution of magnetohydrodynamic flow through duct with perturbated boundary using RBF-FD method". *International Journal of Ambient Energy* 45(1). https://doi.org/10.1080/01430750.2023.2276130.

Sarker, S., Chatzizisis, YS., and Terry, BS. 2020. "Computational optimization of a novel atraumatic catheter for local drug delivery in coronary atherosclerotic plaques". *Medical engineering and physics* 79. 26-32.

Shafi Ullah Siddiqui, and Chhama Awasthi,2017. "Mathematical Analysis on Pulsatile Flow through a Catheterized Stenosed Artery" *Journal of Applied Mathematics and Physics* 5(9). 10.4236/jamp.2017.59157.

Shaikh, F., Shaikh, A., Hinçal, E., and Qureshi, S.2023. "Comparative analysis of numerical simulations of blood flow through the segment of an artery in the presence of stenosis". *Journal of Applied Mathematics and Computational Mechanics* 22. 49-61.

Srivastava, V., and Rastogi, R., 2010. "Blood flow through a stenosed catheterized artery: Effects of hematocrit and stenosis shape" *Computers and Mathematics with Applications* 59. 1377-1385.

Tian, X., Sun, A., Liu, X., Pu, F., Deng, X., Kang, H., and Fan, Y. 2016. "Influence of catheter insertion on the hemodynamic environment in coronary arteries". *Medical Engineering and Physics* 38. 10.1016/j.medengphy.2016.06.013.

Tomaszewski, M., Sybilski, K., Baranowski, P., and Małachowski, J. 2020. "Experimental and numerical flow analysis through arteries with stent using particle image velocimetry and computational fluid dynamics method", *Biocybernetics and Biomedical Engineering* 40(2). 740-751